

Strain-relieved $\text{Ba}_{0.6}\text{Sr}_{0.4}\text{TiO}_3$ thin films for tunable microwave applications

Wontae Chang,^{a)} Steven W. Kirchoefer, Jeffrey M. Pond, and James S. Horwitz
Naval Research Laboratory, 4555 Overlook Avenue SW, Washington, DC 20375

Louise Sengupta
Paratek Microwave, Inc., 6935-N Oakland Mills Road, Columbia, Maryland 21045

(Received 26 February 2002; accepted for publication 16 May 2002)

This article discusses tunable dielectric thin films, with particularly emphasis on strain-relieved and defect-reduced tunable dielectric thin films that significantly reduce dielectric loss at microwave frequencies. $\text{Ba}_{0.6}\text{Sr}_{0.4}\text{TiO}_3$ (BST) thin films ($\sim 0.3 \mu\text{m}$ thick) were deposited onto (100) MgO single crystalline substrates by pulsed laser deposition at 750°C and 200 mTorr O_2 with a nominal 600-Å-thick BST buffer layer. These films were observed to be strain relieved and show better dielectric properties by exhibiting a significantly high dielectric Q ($= 1/\tan \delta > 100$) while retaining a useful dielectric tuning ($= [C(0) - C(23 \text{ V}/\mu\text{m})]/C(0) > 20\%$, where C is the film capacitance) at 8 GHz compared to strained BST thin films. The BST buffer layer could be composed of any porous BST phase with randomly oriented grains between a nearly amorphous phase and a fully crystalline phase. A further increase in the dielectric Q was observed in strain-relieved BST thin films mixed with MgO and strain-relieved BST thin films doped with W. © 2002 American Institute of Physics. [DOI: 10.1063/1.1491996]

I. INTRODUCTION

$\text{Ba}_x\text{Sr}_{1-x}\text{TiO}_3$ (BST) ($0 \leq x \leq 1$) is a solid solution ferroelectric material exhibiting a large dielectric constant change with applied dc electric field.¹ The dc electric field dependent dielectric constant is currently being used to develop tunable microwave devices, such as voltage-controlled oscillators, tunable filters, and phase shifters.²⁻⁴ The availability of tunable microwave devices based on ferroelectric thin films would reduce the size and operating power of devices while providing wide bandwidth and narrow beam width. A large electric field effect has already been demonstrated in ferroelectric thin films.⁵ In addition to the dielectric constant tunability with applied dc electric field, another critical dielectric property in tunable microwave applications is the dielectric Q ($= 1/\tan \delta$). Although many efforts have been made to understand the origin of the dielectric loss, conventional tunable dielectric materials, both bulk ceramics and thin films, show too low of a dielectric Q to be useful for many microwave device applications. A dielectric $Q > 200$ will be required for many tunable microwave applications.

One of significant factors affecting the microwave dielectric properties is the structural distortion caused by film strain, which enhances the inverse relationship between dielectric tuning and dielectric Q .⁶⁻⁹ The inverse relationship results in either large dielectric tuning ($> 75\%$) with low dielectric Q (< 50) or small dielectric tuning ($< 10\%$) with high dielectric Q (> 200) for a reasonably small dc bias voltage (i.e., 50 V) and gap size (i.e., $5 \mu\text{m}$) of planar capacitors at microwave frequencies, depending on either in-plane tetragonal distortion ($a_{\parallel} > a_{\perp}$), where a_{\parallel} and a_{\perp} are in-plane

and normal lattice parameters of film or normal tetragonal distortion ($a_{\parallel} < a_{\perp}$), respectively. Therefore, as far as a strain-induced structural distortion exists in the film, the microwave dielectric properties of the film can never exhibit both large dielectric tuning and high dielectric Q at the same time, and relief of film strain should result in improved dielectric properties. In this article, a method for making tunable dielectric thin films having substantially higher dielectric Q while keeping reasonable dielectric tuning at microwave frequencies as compared to conventional dielectric thin films is presented. This method forms a strain-relieved dielectric thin film, thereby minimizing the effect of the inverse relationship.

II. EXPERIMENT

$\text{Ba}_{0.6}\text{Sr}_{0.4}\text{TiO}_3$ (BST) thin films ($\sim 0.3 \mu\text{m}$ thick) have been deposited onto (100) MgO single crystalline substrate at 750°C in an oxygen ambient pressure of 200 mTorr by pulsed laser deposition (PLD) under three different processing conditions: (i) without a buffer layer, (ii) with a nominal 200-Å-thick BST buffer layer, and (iii) with a nominal 600-Å-thick BST buffer layer. The thin (≤ 1000 -Å-thick) BST buffer layer was deposited on a (100) MgO substrate at room temperature and 200 mTorr O_2 by PLD. The microstructure of the BST buffer layer can be modified into any phase from a nearly amorphous phase to a randomly oriented fully crystalline phase, depending on an in-PLD chamber heat treatment following the room temperature deposition. Also, 1.0, 20.0, and 60.0 wt. % MgO-mixed $\text{Ba}_{0.6}\text{Sr}_{0.4}\text{TiO}_3$ thin films and 1.0 mol. % W-doped $\text{Ba}_{0.6}\text{Sr}_{0.4}\text{TiO}_3$ thin films were grown on (100) MgO substrates at 750°C and 200 mTorr O_2 with nominal 600-Å-thick BST buffer layers. The PLD system used to grow the BST films has been described

^{a)} Author to whom correspondence should be addressed; electronic mail: chang@ccs.nrl.navy.mil

previously.^{10,11} The output of a short-pulsed (30 ns full width at half maximum) excimer laser operating with KrF ($\lambda=248$ nm) at a repetition rate of 5 Hz was focused to a spot size of ~ 0.1 cm² and an energy density of ~ 1.9 J/cm² onto a BST-based PLD ceramic target (i.e., Ba_{0.6}Sr_{0.4}TiO₃, MgO-mixed Ba_{0.6}Sr_{0.4}TiO₃, or W-doped Ba_{0.6}Sr_{0.4}TiO₃ bulk ceramics, that were 2 in. in diameter and 0.25 in. thick). The vaporized material was deposited onto a substrate approximately 5 cm away from the target. All the deposited films were postannealed in flowing O₂ at 1000 °C for 6 h. X-ray diffraction (XRD) and scanning electron microscopy (SEM) were used for film structure and surface morphology characterization.

Single-gap planar capacitors with gaps from 5 to 20 μ m were deposited on top of the BST thin films through a photolithograph liftoff process by *e*-beam evaporation of 0.5 μ m thick Au with a thin layer of Ti for adhesion. Interdigitated capacitors with gaps from 6 to 12 μ m were also deposited on top of the BST films through a polymethylmethacrylate liftoff mask by *e*-beam evaporation of 1.5 μ m thick Ag with an adhesive thin layer of Cr and a protective thin layer of Au. The microwave dielectric properties, capacitance, and dielectric Q ($=1/\tan \delta$), of BST thin films were characterized with two different techniques in this article: (i) resonance curve (S_{21}) measurements using single-gap planar capacitors containing BST thin films incorporated with a half-wavelength ($\lambda/2$) stripline resonator^{12,13} and (ii) reflection curve (S_{11}) measurements using interdigitated capacitors based on BST thin films probed by a 200 μ m pitch Picoprobe microwave probe, which are connected to an HP 8510C network analyzer.^{14,15} From resonance curve (S_{21}) measurements, the capacitance and dielectric Q ($=1/\tan \delta$) of the single-gap planar capacitor were determined from a resonance condition of the half-wavelength stripline resonator incorporating the single-gap planar capacitor, and from a Q correlation between the unloaded Q of the resonator containing the single-gap planar capacitor of BST film and the unloaded Q of the resonator with a nearly lossless capacitor (i.e., Al₂O₃, TiO₂, and CaTiO₃).¹³ It is noted that dielectric Q measurements using a stripline resonator are bounded by the unloaded Q (Q_0) of the resonator with a capacitor practically without dielectric losses (i.e., $Q_0=300$ and 500 for 2 and 8 GHz resonators in this experiment). From reflection curve (S_{11}) measurement, the data were fitted to a parallel resistor-capacitor model to determine capacitance and dielectric Q of the films.^{14,15} The dielectric constant of the films was extracted from the capacitance and the planar capacitor dimensions through conformal mapping techniques for single-gap planar capacitors¹⁶ and for interdigitated capacitors.¹⁷

III. RESULTS AND DISCUSSION

A. Film structure and surface morphology

Figure 1 shows θ - 2θ XRD scans for Ba_{0.6}Sr_{0.4}TiO₃ thin films (~ 0.3 μ m thick) deposited onto (100) MgO single crystalline substrates by PLD at 750 °C and 200 mTorr O₂ under three different processing conditions: (i) without a buffer layer [Fig. 1(a)], (ii) with a nominal 200-Å-thick BST buffer layer [Fig. 1(b)], and (iii) with a nominal 600-Å-thick BST buffer layer [Fig. 1(c)]. The BST films in Figs. 1(a) and

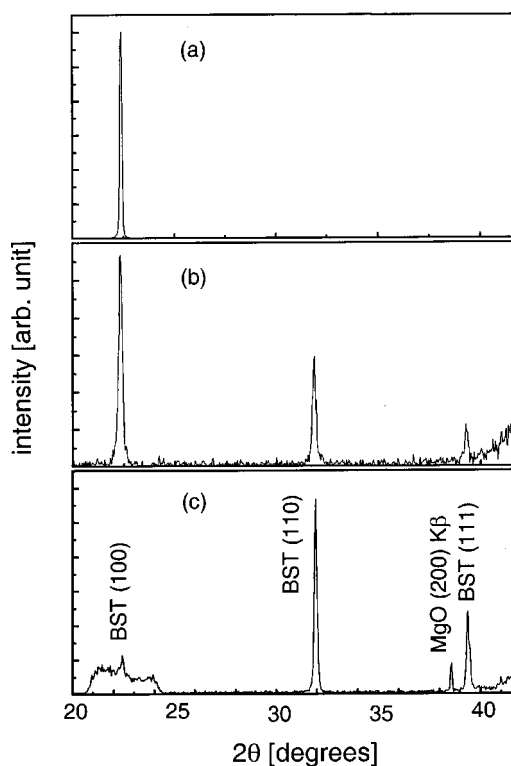


FIG. 1. XRD patterns of BST thin films deposited on (001) MgO (a) without a buffer layer, (b) with a 200-Å-thick BST buffer layer, and (c) with a 600-Å-thick BST buffer layer.

1(b) can be considered as predominantly (100) oriented films if their diffraction intensities are compared to those of randomly oriented powder diffraction peaks [i.e., I_{110}/I_{100} is about 9, where I_{110} and I_{100} are the XRD intensity for (110) and (100) planes of a randomly oriented BST phase].¹⁸ For these (100)-oriented BST films [Figs. 1(a) and 1(b)], the lattice parameters along the surface normal (a_{\perp}) and in the plane of the films (a_{\parallel}) were determined from XRD patterns of symmetric (004) or (002) and asymmetric (024) reflections (Figs. 2 and 3). The difference in the normal lattice parameter a_{\perp} obtained from (004) and (002) is typically less than 0.0005 Å. In cases where the XRD peak intensity from BST films is not clear enough to determine the peak position, the XRD summation mode was used as shown in Fig. 3. Diffraction peaks from the MgO substrate were used as an internal standard to reduce errors associated with measurement. Each BST diffraction peak was fitted with two Gaussian functions by considering four factors of peak shape (the ratios of height, width, and area of $K\alpha_1$ and $K\alpha_2$ peaks, and the distance between $K\alpha_1$ and $K\alpha_2$ peaks) after removing the background. The uncertainty of the lattice parameter is typically less than 0.001 Å.

The lattice parameters of the BST thin films calculated from an analysis of the XRD data are presented in Table I. The in-plane lattice parameter of a BST thin film deposited directly on a (001) MgO substrate without a BST buffer layer is observed to be 0.2% larger than the normal lattice parameter, resulting in an in-plane tetragonal lattice distortion ($a_{\parallel} > a_{\perp}$). The in-plane lattice parameter of a BST thin film with a nominal 200-Å-thick BST buffer layer is observed to be

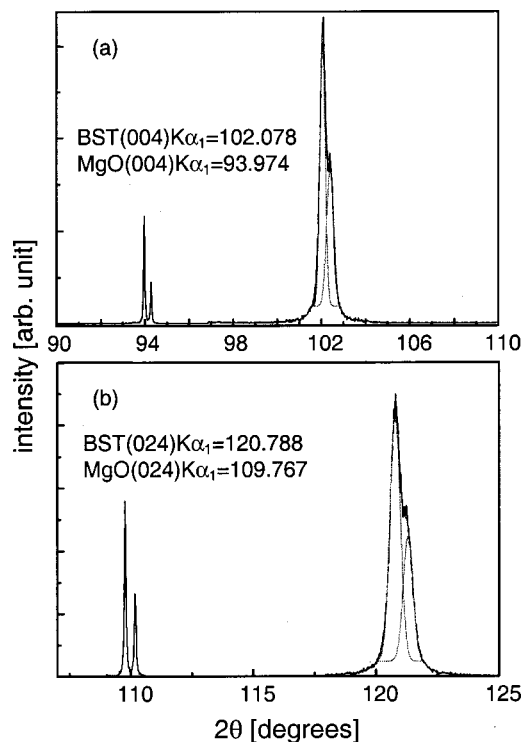


FIG. 2. XRD patterns of: (a) symmetric (004) peaks and (b) asymmetric (024) peaks of BST thin films deposited on (001) MgO at 750 °C and 200 mTorr O₂ and annealed at 1100 °C for 6 h in flowing O₂.

0.2% smaller than the normal lattice parameter, resulting in a normal tetragonal lattice distortion ($a_{\parallel} < a_{\perp}$), although the structure for the corresponding bulk BST should be cubic at room temperature. The film distortion is believed to be due to lattice and thermal expansion mismatches between the film and substrate and due to oxygen vacancies. During film deposition and postannealing processes, the film lattice structure could be modified to minimize the interface energy, which is dominated by the lattice and thermal expansion mismatches between the film and substrate. Oxygen vacancies, mostly formed during film deposition, were observed to significantly affect the film lattice structure by causing either an in-plane or normal lattice distortion (i.e., $a_{\parallel} > a_{\perp}$ or $a_{\parallel} < a_{\perp}$) depending on oxygen deposition pressure.¹⁹ This preferentially directional lattice could be due to an oxygen–vacancy preferential direction, either in-plane or normal, depending on the oxygen deposition pressure in conjunction with the film deposition direction. In the case of a BST thin film with a nominal 200-Å-thick BST buffer layer, the buffer layer, which was expected to form a dispersed small BST phase on MgO substrate, caused the film lattice structure to be modified into a normal tetragonal lattice distortion ($a_{\parallel} < a_{\perp}$), which is different from the in-plane tetragonal lattice distortion ($a_{\parallel} > a_{\perp}$) observed in BST films deposited without the buffer layer. Presumably, this is because the nominal BST buffer layer may affect not only the film relaxation from the lattice mismatch and thermal expansion mismatch but also the film lattice expansion from preferentially directed oxygen vacancies (i.e., in-plane lattice expansion for BST films deposited at the oxygen deposition pressure of 200 mTorr as in this study).

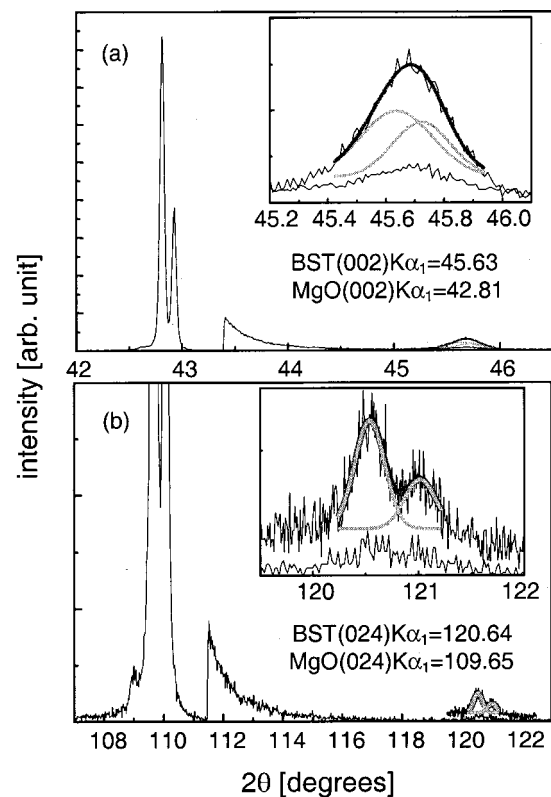


FIG. 3. XRD patterns of (a) symmetric (002) peaks and (b) asymmetric (024) peaks of BST thin films deposited on (001) MgO with a 200-Å-thick BST buffer layer and annealed at 1100 °C for 6 h in flowing O₂. Insets show $K\alpha_1$ and $K\alpha_2$ peak fittings for BST peaks obtained from XRD summation mode.

An analysis of the XRD pattern of Fig. 1(c) indicates the BST thin film deposited with a 600-Å-thick BST buffer layer is of a single perovskite phase but does not have a preferred orientation. The ratio of peak intensities of Fig. 1(c) is very close to the corresponding powder diffraction pattern, indicating that this BST thin film is in a randomly oriented polycrystalline phase. The lattice structure of this BST film was determined to be a cubic phase ($a_0 = 3.966$ Å) by analyzing five XRD reflection peaks from the BST film [i.e., (100), (110), (111), (200) and (211)] using a least square method. It is also noted that the lattice parameter (3.966 Å) of this BST thin film is very close to the equilibrium lattice parameter (3.965 Å) of the corresponding bulk BST.¹⁸ Figure 4 shows that the randomness of film orientation originates from the buffer layer. Figure 4(a) shows a XRD pattern of the BST buffer layer whose SEM image is shown in Fig. 5(g), which is deposited at room temperature with a nominal thickness of 1000 Å and then heated to the substrate temperature of 750 °C for 1 min in an oxygen background pressure of 200 mTorr. The microstructure of this film turns out to be almost amorphous with an extremely small size of perovskite BST phase nucleation. Figure 4(b) shows an XRD pattern of the BST buffer layer whose SEM image is shown in Fig. 5(h), which is deposited at room temperature with a nominal thickness of 1000 Å and then annealed at 900 °C for 6 h in an oxygen background pressure of 1 atm. The microstructure of this film is fully crystalline. The XRD patterns for both BST buffer layers with nearly amorphous and fully crystalline

TABLE I. Lattice parameters of three types of BST thin films.

BST films with/without a BST buffer layer	Lattice parameter (\AA)	
	in-plane (a_{\parallel})	normal (a_{\perp})
BST film without a buffer layer	3.969	3.962
BST film with a 200- \AA -thick BST buffer layer	3.957	3.966
BST film with a 600- \AA -thick BST buffer layer	3.966	

phases are very close to the corresponding powder diffraction pattern as shown in Fig. 4(c). It is possible to design the microstructure of a BST buffer layer to be any phase between nearly amorphous and fully crystalline.

Figure 5 shows SEM images of: (a) as-deposited and (b) annealed BST films without a buffer layer, (c) as-deposited and (d) annealed BST films with a 200- \AA -thick BST buffer layer, (e) as-deposited and (f) annealed BST films with a 600- \AA -thick BST buffer layer, (g) a nearly amorphous BST buffer layer, and (h) a fully crystalline BST buffer layer. As shown in Fig. 5, BST films with a BST buffer layer have a rough surface due to the randomly oriented grain morphology as compared to BST films without a buffer layer. The morphologies of both buffer layers shown in Figs. 5(g) and 5(h) show relatively large voids between the BST grains (i.e., extremely small or big grains), and presumably the randomly oriented grains in the buffer layer could serve as seeds for the subsequently deposited crystalline BST film. The random orientation of the grains and the voids between the grains in the buffer layer could help to not only relieve film strain but also grow crystalline grains in the subsequently deposited dielectric film. The SEM images of as-deposited BST films

with a BST buffer layer shown in Figs. 5(c) and 5(e) show that the regions of the voids in the buffer layer are filled with an aggregation of small grains ($\leq 0.1 \mu\text{m}$) during the film deposition at a high temperature (i.e., 750°C). After a post-deposition anneal, the grain size is observed to increase significantly up to a size of $\sim 0.5 \mu\text{m}$ by reducing grain boundaries which preexisted in the as-deposited BST films, as shown in Figs. 5(d) and 5(f).

These structural (i.e., lattice structure and microstructure) analyses indicate that BST film strain due to the film-substrate mismatches (i.e., lattice and thermal expansion) could be effectively avoided using an optimized BST buffer layer during film deposition and postannealing processes. Thus, optimal annealing effects (i.e., reducing defects and growing grains) can be achieved without thermally induced film strain due to the film-substrate thermal expansion mismatch.

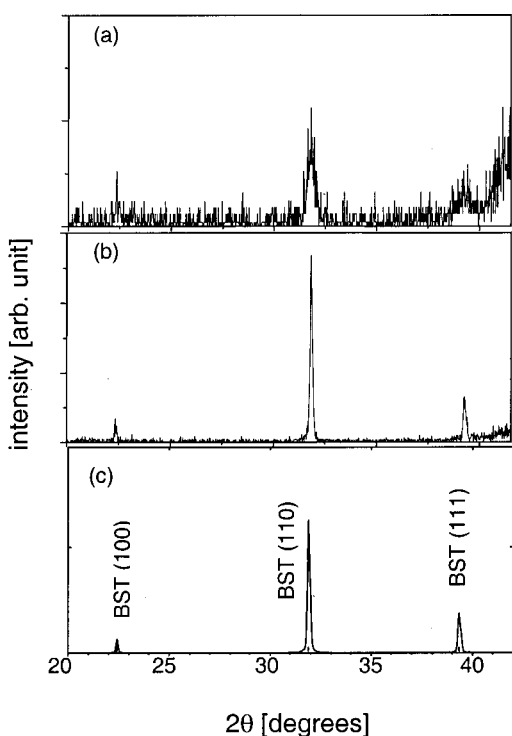


FIG. 4. XRD patterns of (a) and (b) BST buffer layer [using the same film as in Figs. 5(g) and 5(h), respectively], and (c) JCPDS card #34-0411 for $\text{Ba}_{0.6}\text{Sr}_{0.4}\text{TiO}_3$ powder.

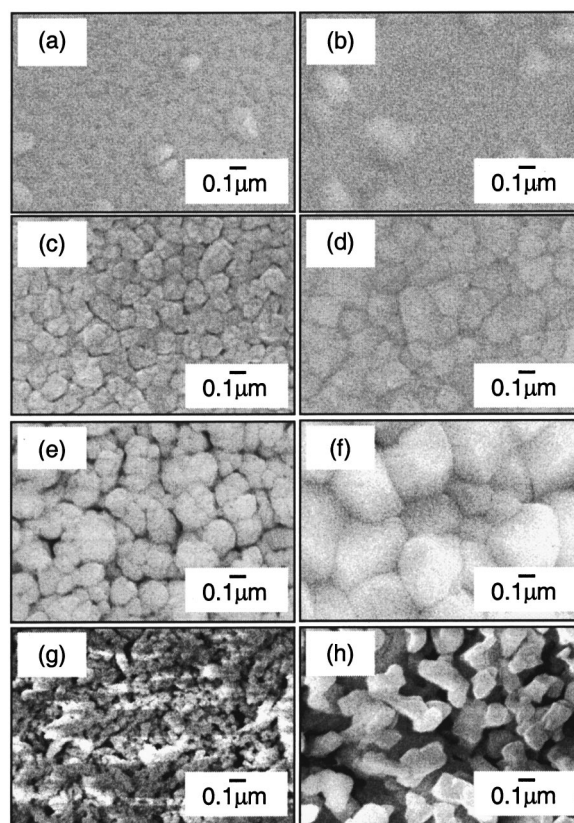


FIG. 5. SEM images of: (a) as-deposited and (b) annealed BST film without a buffer layer, (c) as-deposited and (d) annealed BST film with a 200- \AA -thick BST buffer layer, (e) as-deposited, and (f) annealed BST film a 600- \AA -thick BST buffer layer, (g) nearly amorphous BST buffer layer and (h) fully crystalline BST buffer layer.

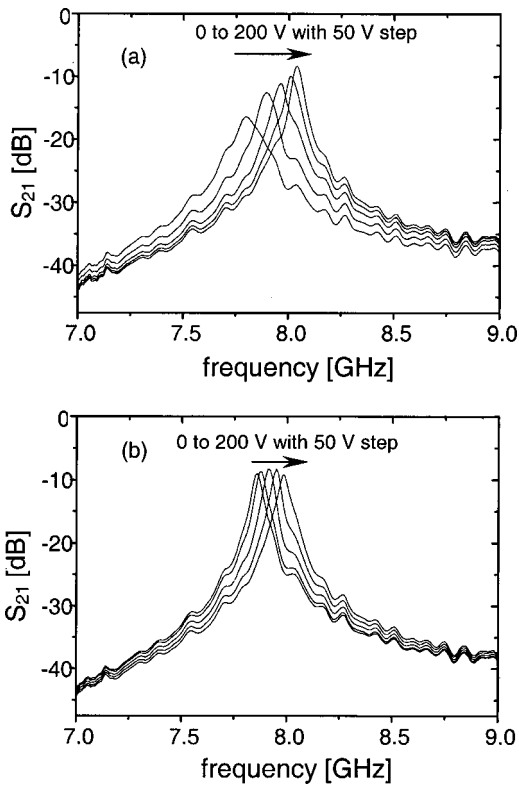


FIG. 6. Resonance curves (S_{21}) of a stripline resonator incorporating single-gap planar capacitors of (a) strained ($a_{\parallel} > a_{\perp}$) and (b) strain-relieved BST films at different applied dc bias voltages up to 200 V at room temperature.

B. Microwave dielectric properties

Figures 6 and 7 show typical resonance transmission (S_{21}) and reflection (S_{11}) measurements of planar capacitors containing strained ($a_{\parallel} > a_{\perp}$) and strain-relieved BST thin films at different applied dc bias voltages at room temperature, respectively. The resonance and reflection curves for strain-relieved BST thin films are observed to be significantly different from those for strained ($a_{\parallel} > a_{\perp}$) BST thin films in terms of the peak height (S_{21}) and 3 dB width (Δf) of the resonance and in terms of the reflection curve position with respect to the outer boundary of the Smith chart for the reflection measurements. The resonance peaks for strain-relieved BST films show less dependence on applied dc bias voltage [Fig. 6(b)], while the peaks of strained ($a_{\parallel} > a_{\perp}$) BST thin films have a clear dc dependence by exhibiting higher insertion loss (S_{21}) and broader 3 dB width (Δf) at lower dc voltages [Fig. 6(a)]. Also, the reflection curves, measured at 0 and 40 V on the Smith chart for strain-relieved BST films, appear very close to the outer boundary of the Smith chart, which corresponds to a low loss capacitance [Fig. 7(b)]. The curves of strained ($a_{\parallel} > a_{\perp}$) BST thin films show a dc dependence and the curve measured at 0 V appear further away from the outer boundary of the Smith chart, which indicates that the capacitor has greater loss [Fig. 7(a)]. The observed differences in insertion loss S_{21} , 3 dB width Δf , and reflection loss S_{11} between strained ($a_{\parallel} > a_{\perp}$) and strain-relieved BST films are directly related to the differences in dielectric loss ($\tan \delta$) of the films.^{13–15} Another difference in the measurements between strain-relieved and

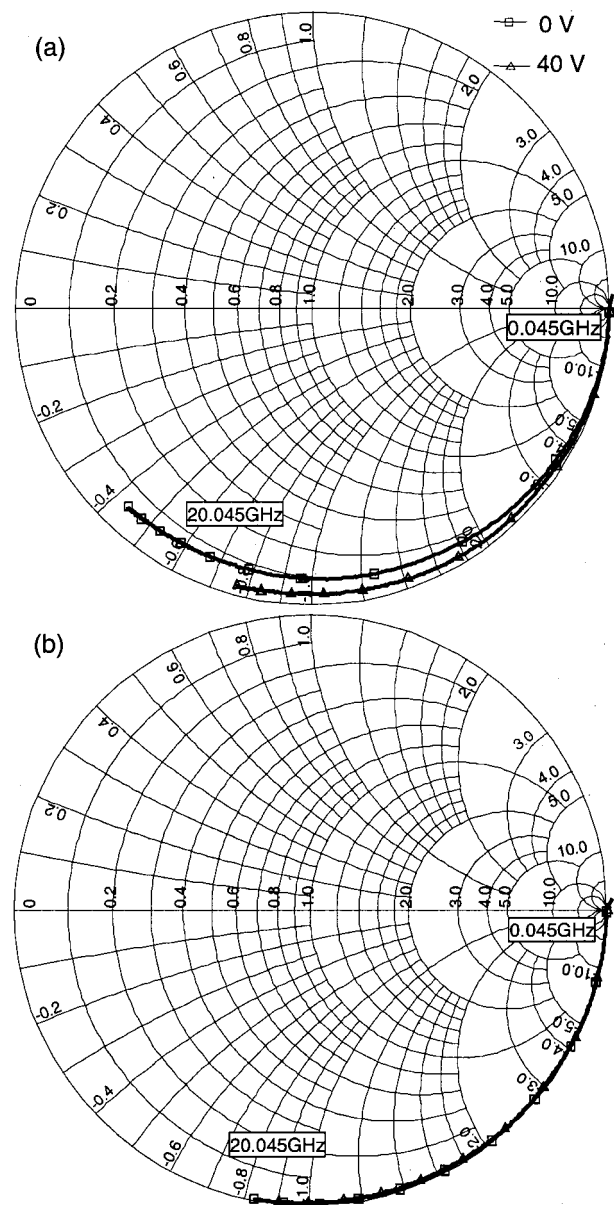


FIG. 7. Reflection curves (S_{11}) on the Smith chart for interdigitated capacitors of BST films grown (a) strained ($a_{\parallel} > a_{\perp}$) and (b) strain-relieved BST films at 0 and 40 V bias over the frequency range from 0.045 to 20.045 GHz at room temperature.

strained ($a_{\parallel} > a_{\perp}$) BST thin films is observed in terms of the resonance peak position or the reflection curve length at 0 V, which are determined by the capacitance (or the dielectric constant), and in terms of the range of resonance frequency shift or the difference in reflection curve length with dc bias voltages, which corresponds to the dielectric tuning, as shown in Figs. 6 and 7. All the differences in resonance curves S_{21} and reflection curves S_{11} of planar capacitors containing strained ($a_{\parallel} > a_{\perp}$) and strain-relieved BST thin films come from the differences in the dielectric properties of the films, which are originated by the differences in the film strain.

Typical in-plane film dielectric constants for $a_{\parallel} > a_{\perp}$ strained, strain-relieved, and $a_{\parallel} < a_{\perp}$ strained BST thin films

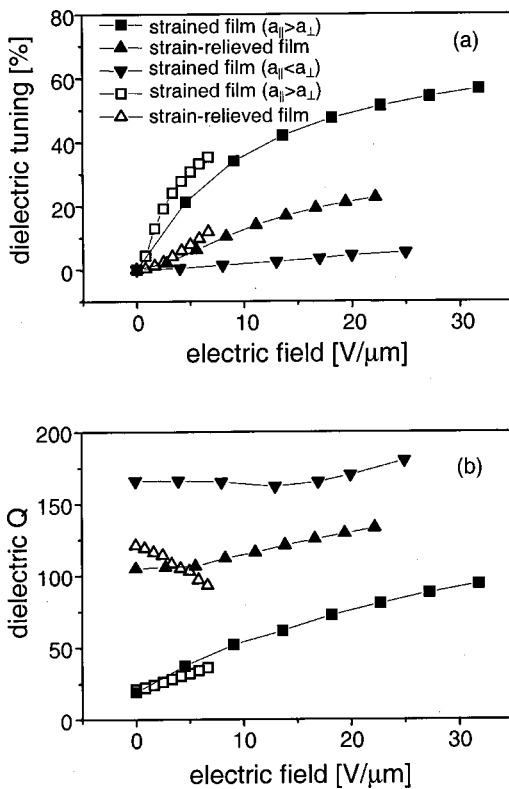


FIG. 8. (a) Dielectric tuning and (b) dielectric Q of strained and strain-relieved BST thin films as a function of applied dc electric field. The black and white data points were obtained from S_{21} measurements at 8 GHz and from S_{11} measurements at 10 GHz, respectively.

as shown in Table I were observed to be 800, 500, and 300, respectively. Figure 8 shows the dielectric tuning of capacitance C , defined as $[C(0) - C(V_{dc})]/C(0)$, and dielectric $Q (= 1/\tan \delta)$ of strained ($a_{||} > a_{\perp}$ and $a_{||} < a_{\perp}$) and strain-relieved BST thin films as a function of applied dc electric field. The strain-relieved BST films exhibit a relatively high dielectric Q_{0V} (~ 100) with a reasonably good dielectric tuning ($\sim 20\%$ at $20 \text{ V}/\mu\text{m}$). The strained BST films show either high dielectric tuning ($\sim 50\%$ at $25 \text{ V}/\mu\text{m}$) with a low dielectric Q_{0V} (~ 20) or high dielectric Q_{0V} (> 150) with a low dielectric tuning ($\sim 5\%$ at $25 \text{ V}/\mu\text{m}$), depending on the film strain, $a_{||} > a_{\perp}$ or $a_{||} < a_{\perp}$, respectively. Most film strains due to lattice mismatch and oxygen vacancies are thought to be relieved in such a way as to minimize the film energy (i.e., the interface energy between the film and substrate and the film bulk energy) during the postannealing process. However, as far as BST films are strained due to thermal expansion mismatch between the film and substrate during the postannealing process, the films cannot have desirable dielectric properties exhibiting both high dielectric Q and high dielectric tuning because of the film strain, even though structural defects are significantly reduced and crystalline grains are largely grown in the film during the postannealing process. For example, Dimos *et al.* show that reduction in loss is realized by dramatically increasing the grain size of the dielectric films.²⁰ The increase in grain size is realized by heating the film to a temperature at which the grains experience regrowth. However, after postannealing, the Q value at 0 V_{dc} of the epitaxial dielectric films grown on LaAlO_3 sub-

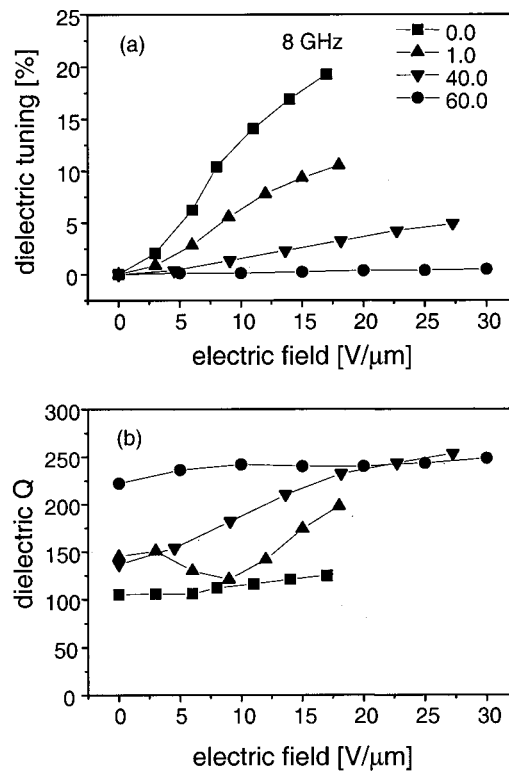


FIG. 9. (a) Dielectric tuning and (b) dielectric Q of strain-relieved BST thin films mixed with MgO (0.0, 1.0, 40.0, and 60.0 wt %) as a function of applied dc electric field. The data were obtained from S_{21} measurements at 8 GHz.

strates are even lower ($Q_{0V} = 30$) with higher dielectric tuning ($64\% - 69\%$ at $E = 3 - 5 \text{ V}/\mu\text{m}$) at 1–2 GHz than the films without postannealing (i.e., $Q_{0V} = 40 - 50$ with a $36\% - 38\%$ dielectric tuning). Presumably, the resulting dielectric properties result because, after postannealing, the epitaxial films are strained further into an in-plane tetragonal distortion due to thermal expansion mismatch between the film and substrate, even though film grains are expected to regrow during the postannealing process. As shown in Fig. 8, strain-relieved BST thin films using an optimized BST buffer layer are free to be heat treated without a thermally induced structural distortion caused by film strain due to thermal expansion mismatch during the postannealing process, and therefore have only a desirable annealing effect (i.e., reducing defects and growing grains). The strain-relieved and defect-reduced BST films exhibit much better dielectric properties at high frequencies (i.e., $\geq 2 \text{ GHz}$) compared to conventional BST films that could be defect reduced but still strained.

A further increase in the dielectric Q was observed in strain-relieved BST thin films mixed with MgO and strain-relieved BST thin films doped with W. Figure 9 shows the dielectric tuning and dielectric Q of strain-relieved BST thin films mixed with MgO (0.0, 1.0, 40.0, and 60.0 wt %) as a function of applied dc electric field. The data were obtained from S_{21} measurements at 8 GHz. The strain-relieved BST film mixed with 1.0 wt % MgO shows a further increase in the dielectric Q_{0V} (~ 150) with a less dielectric tuning ($\sim 10\%$ at $15 \text{ V}/\mu\text{m}$) compared to the strain-relieved BST

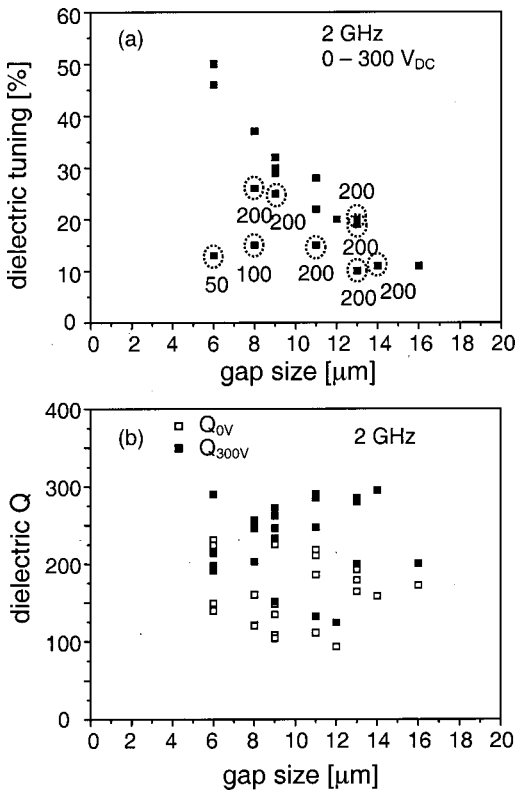


FIG. 10. (a) Dielectric tuning and (b) dielectric Q of strain-relieved BST thin films doped with W (1 mol %) as a function of varactor gap size at applied dc bias voltages up to 300 V. The data were obtained from S_{21} measurements at 2 GHz.

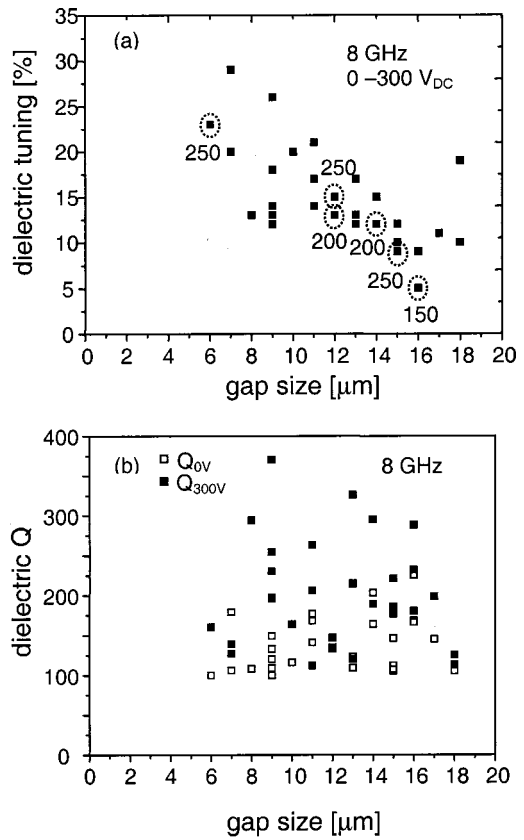


FIG. 11. (a) Dielectric tuning and (b) dielectric Q of strain-relieved BST thin films doped with W (1 mol %) as a function of varactor gap size at applied dc bias voltages up to 300 V. The data were obtained from S_{21} measurements at 8 GHz.

film. However, the strain-relieved BST films mixed with 40.0 and 60.0 wt % MgO show an extremely small dielectric tuning ($<5\%$ at $25 \text{ V}/\mu\text{m}$) although their dielectric Q s are relatively quite high. More measurements of small signal microwave properties of single-gap planar capacitor containing strain-relieved BST thin films doped with 1 mol % W were made as a function of capacitor gap size ranging from 6 to 18 μm . Figures 10 and 11 are plots of dielectric tuning and dielectric Q of strain-relieved BST thin films doped with 1 mol % W as a function of capacitor gap size at applied dc bias voltages up to 300 V except for the circled data points with $V_{\text{MAX}}=50\text{--}250 \text{ V}_{\text{dc}}$ as noted in the figure. The data were obtained from S_{21} measurements at 2 and 8 GHz. Trends in the dielectric properties illustrated in Figs. 10 and 11 are further validated by the fact that many of the data points represent data obtained from several different capacitors with the same gap size. While the dielectric tuning at both frequencies, 2 and 8 GHz, tends to increase as the gap size decreases, the dielectric Q does not show any clear trend with gap size and reveals high dielectric Q s independent of the gap sizes for values ranging from 6 to 18 μm , for the strain-relieved BST films doped with 1 mol % W. As shown in Figs. 10 and 11, these state of the art results show that the strain-relieved BST thin films doped with 1 mol % W have a high dielectric Q_{0V} ($Q_{\text{average}} > 150$) with a reasonable dielectric tuning of $\sim 50\%$ at $50 \text{ V}/\mu\text{m}$ at 2 and 8 GHz. Also, as shown in Fig. 12, the strain-relieved BST thin films doped with 1 mol % W show a stable temperature dependence of

the dielectric properties [i.e., the dielectric tuning of capacitance and the dielectric $Q(=1/\tan \delta)$] over $-20\text{--}60 \text{ }^\circ\text{C}$, and can be used for room temperature tunable microwave applications.

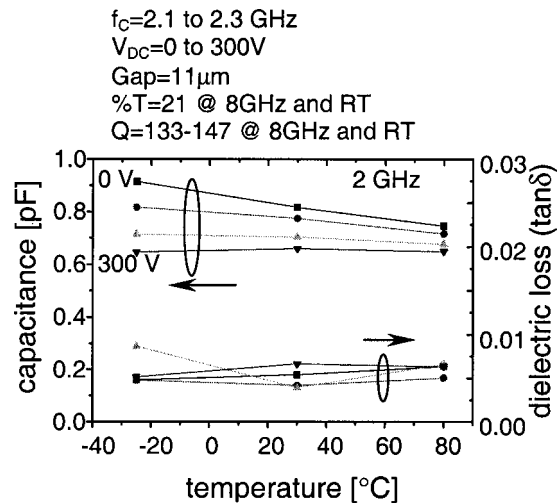


FIG. 12. Capacitance and dielectric loss ($\tan \delta$) of strain-relieved BST thin film doped with W (1 mol %) as a function of temperature at applied dc bias voltages up to 300 V. The data were obtained from S_{21} measurements at 2 GHz. Also, dielectric tuning and dielectric Q of the same BST film measured at 8 GHz and room temperature are noted.

Further work will be performed to reduce the distance between electrodes to less than 1000 Å while preserving the desirable dielectric properties of the strain-relieved BST thin films. This will enable reduction of dc biases to $<10 V_{dc}$ as needed for low voltage tunable microwave applications. This is probably achievable because very thin (<1000 Å) strain-relieved BST films should experience much less interface effect²¹ due to lattice and thermal mismatches between the film and substrate, unlike that which has been observed to significantly degrade the dielectric properties of thin strained BST films.

IV. SUMMARY

The microstructure of BST thin films is observed to be dependent on the presence of a BST buffer layer. BST thin films (~ 0.3 μm thick) deposited onto (100) MgO at 200 mTorr oxygen pressure by PLD without a buffer layer showed a strain-induced in-plane tetragonal distortion ($a_{\parallel} > a_{\perp}$) and the BST films with a nominal 200-Å-thick BST buffer layer showed a strain-induced normal tetragonal distortion ($a_{\parallel} < a_{\perp}$). State of the art results in tunable microwave dielectric properties are observed in the strain-relieved 1 mol% W doped BST thin films with a nominal 600-Å-thick BST buffer layer exhibiting a high dielectric Q_{0v} (~ 100 – 200) with a reasonable dielectric tuning of $\sim 50\%$ at 50 V/μm. A further investigation will be performed to reduce the distance between electrodes to less than 1000 Å while keeping the desirable dielectric properties of the strain-relieved BST thin films.

ACKNOWLEDGMENTS

The authors wish to acknowledge Yongfei Zhu and Xubai Zhang at Paratek Microwave Inc. for helpful assistance for 2 and 8 GHz measurements using gap coupled stripline resonators.

- ¹L. Davis and L. G. Rubin, *J. Appl. Phys.* **24**, 1194 (1953).
- ²C. H. Mueller, R. R. Romanofsky, and F. A. Miranda, *IEEE Potentials* **20**, 36 (2001).
- ³S. S. Gevorgian and E. L. Kollberg, *IEEE Trans. Microwave Theory Tech.* **49**, 2117 (2001).
- ⁴D. S. Korn and H.-D. Wu, *Integr. Ferroelectr.* **24**, 215 (1999).
- ⁵K. R. Carroll, J. M. Pond, D. B. Chrisey, J. S. Horwitz, R. E. Leuchtner, and K. S. Grabowski, *Appl. Phys. Lett.* **62**, 1845 (1993).
- ⁶I. V. Barskii, O. G. Vendik, A. D. Smirnov, and G. S. Khizha, *Sov. Phys. Tech. Phys.* **34**, 1065 (1990).
- ⁷W. Chang, J. S. Horwitz, A. C. Carter, J. M. Pond, S. W. Kirchoefer, C. M. Gilmore, and D. B. Chrisey, *Appl. Phys. Lett.* **74**, 1033 (1999).
- ⁸W. Chang, J. S. Horwitz, W. J. Kim, J. M. Pond, S. W. Kirchoefer, C. M. Gilmore, S. B. Qadri, and D. B. Chrisey, *Integr. Ferroelectr.* **24**, 257 (1999).
- ⁹W. J. Kim, W. Chang, S. B. Qadri, J. M. Pond, S. W. Kirchoefer, D. B. Chrisey, and J. S. Horwitz, *Appl. Phys. Lett.* **76**, 1185 (2000).
- ¹⁰K. S. Grabowski, J. S. Horwitz, and D. B. Chrisey, *Ferroelectrics* **116**, 19 (1991).
- ¹¹J. S. Horwitz, D. B. Chrisey, K. S. Grabowski, and P. E. Leuchtner, *Surf. Coat. Technol.* **51**, 290 (1992).
- ¹²D. Galt, J. C. Price, J. A. Beall, and R. H. Ono, *Appl. Phys. Lett.* **63**, 3078 (1993).
- ¹³A. B. Kozyrev, V. N. Keis, G. Koepf, R. Yandrofski, O. I. Soldatenkov, K. A. Dudin, and D. P. Dovgan, *Microelectron. Eng.* **29**, 257 (1995).
- ¹⁴S. W. Kirchoefer, J. M. Pond, A. C. Carter, W. Chang, K. K. Agarwal, J. S. Horwitz, and D. B. Chrisey, *Microwave Opt. Technol. Lett.* **18**, 168 (1998).
- ¹⁵J. M. Pond, S. W. Kirchoefer, W. Chang, J. S. Horwitz, and D. B. Chrisey, *Integr. Ferroelectr.* **22**, 317 (1998).
- ¹⁶H.-D. Wu, Z. Zhang, F. S. Barnes, C. M. Jackson, A. Kain, and J. D. Cuchiaro, *IEEE Trans. Appl. Supercond.* **4**, 156 (1994).
- ¹⁷S. S. Gevorgian, T. Martinsson, P. I. J. Linner, and E. L. Kollberg, *IEEE Trans. Microwave Theory Tech.* **44**, 896 (1996).
- ¹⁸JCPDS card #34-0411 for Ba_{0.6}Sr_{0.4}TiO₃ powder.
- ¹⁹W. J. Kim, H.-D. Wu, W. Chang, S. B. Qadri, J. M. Pond, S. W. Kirchoefer, D. B. Chrisey, and J. S. Horwitz, *J. Appl. Phys.* **88**, 5448 (2000).
- ²⁰D. B. Dimos, R. W. Schwartz, M. V. Raymond, H. N. Al-Shareef, C. Mueller, and D. Galt, US Patent No. 6,096,127 (2000).
- ²¹S. Trolier-McKinsky, P. Chindaudom, K. Vedam, and R. E. Newman, in *Physics of Thin Films*, edited by K. Vedam (Academic, New York, 1994), Vol. 152, p. 169.